Ground Vehicle Generalized Forces and Moment Governor Design Via Noncertainty-Equivalent Adaptive Prescribed Performance Control

Xingyu Zhou*, Heran Shen*, Zejiang Wang†, Hyunjin Ahn*, Yung-Chi Kung*, and Junmin Wang*

*Walker Department of Mechanical Engineering, University of Texas at Austin, Austin, TX, USA

†Oak Ridge National Laboratory, Oak Ridge, TN, USA

Email: {xingyu.zhou, jwang}@austin.utexas.edu, {hs29354, hjahn, yung-chi.kung}@utexas.edu, wangz2@ornl.gov

***Abstract*— Torque-vectoring technology demonstrates great potential in improving the safety and performance of ground vehicles. In this paper, a novel generalized forces and moment governor for torque vectoring is suggested. The proposed solution strategically combines prescribed performance control, noncertainty equivalent adaptive control design, and a smooth projection operator. The main advantage of the proposed control strategy lies in its capability to guarantee both the transient performance and prompt recovery of the desired deterministic behavior of the closed-loop adaptive system, even in the presence of parametric uncertainties. ASM simulation results are presented to validate the efficacy of the proposed generalized forces and moment governor and to demonstrate its superiority over a baseline solution.**

Keywords—Adaptive Control, Motion Control, Prescribed Performance Control, Smooth Projection, Torque Vectoring

I. INTRODUCTION

A. Background

With the advancement of vehicle actuation and sensing technologies, vehicle motion control systems are continually evolving [1]-[3]. Whereas traditional ground vehicles rely on hand-steering and accelerator/brake pedals to control yaw/lateral and longitudinal motions, next-generation vehicles will incorporate multiple x-by-wire and intelligently controlled subsystems. These subsystems will have overlapping control authorities, leading to fully/redundantly actuated systems with augmented safety and flexibility.

Torque vectoring [1] is a prime example of such redundantly actuated vehicular systems. It allows individual wheels or groups of wheels to receive different levels of driving torque, and when used in conjunction with active steering, has shown significant potential for enhancing the vehicle's safety and performance, particularly under challenging road conditions like sharp turns or slippery surfaces. Moreover, torque vectoring is beneficial to automated/autonomous driving systems, as it can enhance the vehicle's stability and maneuverability in various driving scenarios.

As a *de facto* practice, the control system for torque vectoring adopts a trio-loop hierarchical structure [4], which consists of a high-level generalized forces and moment (GFM) governor responsible for controlling planar vehicle motions, a mid-level control allocation scheme that (optimally) distributes the GFM commands to actuators (e.g., the steering motor), and low-level servo controllers to ensure that the given commands are properly executed. The focus of this paper is on the design of the high-level GFM governor.

B. Literature Overview

Nonlinear control methodologies are commonly used in the design for GFM governors, as the (planar) vehicle dynamic model is inherently nonlinear [1]. In this paradigm, GFM governors can be clustered into two subclasses, one based on nonlinear deterministic robust control (NDRC), and the other based on nonlinear adaptive control (NAC).

The NDRC-based GFM governors are usually designed based on the sliding-mode control technique [1] or the nonlinear composite control method [5]. Although NDRC can provide guaranteed robustness against bounded uncertainties/disturbances, it comes with an intrinsic drawback. Namely, when dealing with large-scale model uncertainties, the NDRC design may generate overly conservative control laws [6]. This conservativeness can lead to excessive control action (so-called the high-gain paradigm), which may not be appropriate for vehicular implementation [7].

On the other hand, another subclass of GFM governors employs the NAC approach, which tackles model uncertainties through online adaptation and learning, thereby sidestepping the conservatism issue in the NDRC design framework. Commonly employed NAC techniques for the GFM governor design include model reference adaptive control [8], adaptive backstepping control [9], and adaptive sliding-model control [10].

C. Research Gaps and Contributions of Our Work

While the aforementioned NAC-based GFM governors have demonstrated their efficacy, there is still considerable room for improving the control system's performance. Our contribution in this paper focuses on three key areas for further enhancements.

First off, the majority, if not all, of NAC-based GFM governors in the literature possess asymptotic stability and signal convergence properties at best. However, transient behaviors, which are equally if not more important than their steady-state counterpart, are often overlooked. Consequently, existing adaptive GFM governors may exhibit inadequate transient performance, such as slow tracking-error convergence, oscillatory responses, and substantial overshoots. This paper aims to address this research gap by formulating an adaptive GFM governor with prescribed performance control (PPC) [11][16]. In a nutshell, the

proposed adaptive PPC solution will guarantee the forward invariance of tracking errors inside certain prespecified funnels (usually exponentially convergent).

Second, virtually all existing adaptive GFM governors are based on the standard certainty-equivalent (CE) adaptive control principle, which has a potential concern of degrading closed-loop performance during adaptation [12]. As a radical departure, this paper proposes to address this issue by adopting the noncertainty equivalent (NCE) adaptive control design method. In contrast to the CE scheme, the NCE method can guarantee prompt recovery of the ideal determinist closed-loop behaviors, which ultimately leads to improved transient performance [13].

Third, some previous studies employed the projection operator to ensure the boundedness of control parameters during online adaptation [4], but the projection operators used were generally discontinuous and, at best, Lipschitz continuous [14]. This may induce non-smooth control laws which can be troublesome for low-level servomechanisms and/or adversely excite unmodelled high-frequency dynamics. In such a respect, this paper will introduce a novel smooth projection operator and integrate it into the parameter adaptation mechanism.

D. Paper Organization

The structure of this paper is organized as follows: Section II establishes the theoretical basis for the design of the control system. Section III outlines the design of the control-oriented model and the adaptive generalized forces and moment (GFM) governor. Section IV presents the numerical results from the dSPACE-ASM simulation study. Finally, Section V serves as the conclusion for this paper.

II. THEORETICAL FOUNDATION

A. Control-Oriented Model

For the scope of this paper, a class of first-order, nonlinear, single-input, parametrically uncertain, dynamic systems in the following form ($x, u \in \mathbb{R}$) is considered:

$$\dot{x} = \sum_{i=1}^{N} a_i f_i(x, w) + bu, \tag{1}$$

where $w \in \mathbb{R}^m$ is a measurable exogenous vector, $f_i(\bullet,\bullet): \mathbb{R} \times \mathbb{R}^m \to \mathbb{R}$ are known continuously differentiable regressor functions. Besides, $a_i \in \mathbb{R}$ and $b \in \mathbb{R}$ are unknown parameters that are constant or slow-time-varying. We make the further assumption that b is non-zero and its sign is known within the system's operating range, in order to ensure the controllability of the system. The rudimentary target here is to command the control input u such that x can track a sufficiently smooth and bounded reference trajectory r as closely as possible. In such a respect, one can define the following tracking-error dynamics ($e \triangleq x - r$):

$$\dot{e} = \sum_{i=1}^{N+1} a_i f_i(x, w) + bu, \tag{2}$$

where $a_{N+1} \triangleq 1$ and $f_{N+1}(x, w) = -\dot{r}$ are an additional pair of parameter-regressor. Note that r and its time derivative are absorbed into the exogenous vector w in the above expression. Equation (2) can be further transformed into:

$$\dot{e} = b\left[\sum_{i=1}^{N+1} \theta_i f_i(x, w) + u\right], \tag{3}$$

where $\theta_i \triangleq a_i/b$.

To foster the guaranteed transient convergence for the tracking error e, the PPC scheme is adopted here. To do so, we would like e to strictly stay inside a prescribed funnel throughout its forward evolution in time, namely,

$$\forall t \in \mathbb{R}^+, \varphi_l(t) < e(t) < \varphi_u(t), \tag{4}$$

where $\varphi_u(t) > \varphi_l(t), \forall t \in \mathbb{R}^+$. As a standard practice, $\varphi_u(t)$ and $\varphi_l(t)$ are chosen to be symmetrical ($\varphi_l(t) = -\varphi_u(t) = \varphi(t) \in \mathbb{R}^+$) as well as exponentially convergent [11]. In particular, one can specify:

$$\varphi(t) = (\varphi_0 - \varphi_\infty)\exp(-\kappa t) + \varphi_\infty, \tag{5}$$

where $\varphi_0 > \varphi_\infty \in \mathbb{R}^+$ and $\kappa \in \mathbb{R}^+$ are user-specified constants. By employing this funnel design, the exponential convergence of the transient response of e can be achieved, and its steady-state value can be regulated within a predetermined terminal set.

Remark 1: The minimum undershoot and maximum overshoot of e are constrained by the magnitude of φ_0 ($\sup_{t\in\mathbb{R}^+}|e(t)| \le \varphi_0$), while the corresponding acceptable steady-state error is tunable by the magnitude of φ_∞ ($|e(\infty)| \le \varphi_\infty$). The exponential decay rate of e is determined by the parameter κ. By adjusting the values of φ_0, φ_∞, and κ in $\varphi(t)$, both the transient and steady-state performance of e can be pre-designed. It is important to notice that φ_0 shall be specified such that it is greater than $|e(0)|$. In other words, the initial width of the prescribed funnel is inherently limited by the initial tracking error.

A nonlinear transformation is employed to transform the constrained PPC control problem (as governed by (3) -(4)) into an equivalent unconstrained counterpart. To do so, we introduce the following nonlinear smooth mapping:

$$\tanh(z) = e\varphi^{-1}(t). \tag{6}$$

This mapping is bijective if and only if e strictly stays within the prescribed funnel, i.e., $-\varphi(t) < e < \varphi(t)$. In other words, any constrained e can be uniquely and smoothly mapped to an unconstrained variable $z \in \mathbb{R}$. Thus, z can be expressed as a nonlinear function of e:

$$z = \frac{1}{2}\ln\left(\frac{1 + e\varphi^{-1}(t)}{1 - e\varphi^{-1}(t)}\right), \tag{7}$$

whose domain is the prescribed funnel $|e(t)| < \varphi(t), \forall t \in \mathbb{R}^+$. Differentiating z with respect to time yields,

$$\dot{z} = \frac{1}{1 - e^2\varphi^{-2}(t)}\left(\frac{\dot{e}}{\varphi(t)} - \frac{e\dot{\varphi}(t)}{\varphi^2(t)}\right). \tag{8}$$

By invoking e's dynamics as presented in (3), equation (8) can be further expanded as,

$$\dot{z} = \frac{1}{\left(1 - e^2\varphi^{-2}(t)\right)}\left\{\frac{b[\sum_{i=1}^{N+1}\theta_i f_i(x, w) + u]}{\varphi(t)} - \frac{e\dot{\varphi}(t)}{\varphi^2(t)}\right\}. \tag{9}$$

Equation (9) can be equivalently transformed into,

$$\dot{z} = -kz + b\left[\sum_{i=1}^{N} \theta_i g_i(z, x, w) + u_e\right], \tag{10}$$

where $k \in \mathbb{R}^+$, $u_e \triangleq g_u(x, w)u$ is the transformed input, and,

$$g_u(x,w) \triangleq \frac{1}{\varphi(t)\left(1-e^2\varphi^{-2}(t)\right)}, \tag{11}$$

$$g_i(z,x,w) \triangleq \frac{f_i(x,w)}{\varphi(t)\left(1-e^2\varphi^{-2}(t)\right)}, \forall i \in [\![1,N]\!], \tag{12}$$

$$g_{N+1}(z,x,w) \triangleq \frac{f_{N+1}(x,w)-e\dot{\varphi}(t)\varphi^{-1}(t)+\zeta}{\varphi(t)\left(1-e^2\varphi^{-2}(t)\right)}, \tag{13}$$

where $\zeta = \varphi(t)\left(1-e^2\varphi^{-2}(t)\right)kz$ in (13).

At this point, the equation (10) is referred to as the control-oriented model. Evidently, so long as z remains bounded, the tracking error e will be restricted within the prespecified funnel, and $g_u(z,x,w)$ will be nonzero so the system in (10) retains the controllability. Furthermore, if z is reduced to zero, e will also be zero (the bijective mapping is symmetric about the origin). If θ_i is perfectly known, the feedback-linearizing control law $u_e = -\sum_{i=1}^{N+1}\theta_i g_i(z,x,w)$ can fulfill such an objective, namely, z and e under such a control law will converge to zero exponentially fast. In practice, it is however nearly impossible to achieve the perfect cancellation of uncertainties in θ_i using such an idealized feedback-linearizing law. Accordingly, to achieve the PPC objective in the presence of parametric uncertainties, we will employ a noncertainty-equivalent adaptive control scheme. To begin with, a smooth projection operator will be introduced.

B. Smooth Projection Operator

The control-oriented model in (10) involves uncertain model parameters θ_i. In practice, it is possible to estimate their bounds $[\underline{\theta}_i, \overline{\theta}_i]$ by leveraging certain physical knowledge. This information can then be incorporated into the parameter adaptation mechanism using a smooth projection operator, which could bring about two advantages. First off, the closed-loop adaptive system becomes more robust, as the projection scheme can prevent unbounded parameter drift caused by disturbances or noise. Secondly, the pre-estimated projection bounds confine the admissible region for adapting control parameters. This leads to improved parameter adaptation by avoiding unnecessary parameter learning efforts that occur outside the admissible parameter regions. This paper introduces a smooth projection operator that utilizes the hyperbolic tangent function [15]. This projection operator aims to project an unconstrained parameter $\lambda \in \mathbb{R}$ onto a confined interval $[\underline{\nu}, \overline{\nu}]$,

$$\nu = \Pi_{[\underline{\nu},\overline{\nu}]}(\lambda) = \underline{\nu} + \frac{1}{2}\Delta_\nu(\tanh(\lambda)+1). \tag{14}$$

where and $\Delta_\nu \triangleq \left(\overline{\nu}-\underline{\nu}\right)$. The smooth projection scheme introduced in equation (14) is characterized by three key properties. Firstly, it is infinitely differentiable (C^∞), which sets it apart from conventional projection operators (such as those discussed in [14] and related literature) that only possess finite-order differentiability at best. Secondly, this one-piece operator does not require gradient computation or boundary layer construction, which makes it a conveniently implementable option for practitioners. The third property of the proposed hyperbolic tangent function-based smooth projection operator is that it is more versatile than conventional projection operators. While traditional operators are only compatible with the CE adaptive control scheme, the proposed operator can work with both CE and NCE schemes, allowing for greater flexibility in its application. In what follows, an NCE adaptive PPC strategy based on such a smooth projection scheme will be delineated.

C. Control Law Formulation

An adaptive control strategy aiming to accomplish the PPC objective is proposed as follows:

$$u = -\frac{1}{g_u(x,w)}\sum_{i=1}^{N+1}\hat{\theta}_i g_i(z,x,w). \tag{15}$$

The following algorithms are used to perform real-time adaptations for unknown parameters θ_i:

$$\begin{cases} \hat{\theta}_i = \Pi_{[\underline{\theta}_i,\overline{\theta}_i]}(\alpha_i+\beta_i) \\ \alpha_i = \varsigma_i \mathrm{sgn}(b)\int_0^z g_i(\varsigma,x,w)d\varsigma \\ \dot{\beta}_i = \begin{pmatrix}\frac{\partial\alpha_i}{\partial z} & \frac{\partial\alpha_i}{\partial x} & \frac{\partial\alpha_i}{\partial w}\end{pmatrix}\begin{pmatrix} kz \\ -\dot{x} \\ -\dot{w}\end{pmatrix} \end{cases}, \tag{16}$$

where $\alpha_i, \beta_i \in \mathbb{R}$ are NCE control parameters, $\varsigma_i \in \mathbb{R}_+$ rates of adaptation.

Remark 2: The conventional projection operators used in CE adaptive control design, such as those in [14], can only project the parameters via altering their time-integration process (*i.e.*, ceasing the integration process if parameters are out of their projection bounds). However, the update of α_i in (16) involves an analytical computation that uses a definite integral with respect to the state x instead of time (so-called NCE proportional adaptation), which makes traditional methods nonapplicable here. This is yet another motivation to devise the smooth projection operator in (14), which is capable of modifying the NCE proportional adaptation.

D. Closed-loop Stability Analysis

To begin with, errors due to the control parameters' adaptation ($\tilde{\theta}_i \triangleq \hat{\theta}_i - \theta_i$) can be parametrized in terms of α_i, β_i, and γ_i:

$$\begin{aligned}\tilde{\theta}_i &= \Pi_{[\underline{\theta}_i,\overline{\theta}_i]}(\alpha_i+\beta_i) - \Pi_{[\underline{\theta}_i,\overline{\theta}_i]}(\gamma_i) \\ &= \frac{1}{2}\Delta\theta_i[\tanh(\alpha_i+\beta_i)-\tanh(\gamma_i)],\end{aligned} \tag{17}$$

where $\gamma_i \triangleq \Pi^{-1}_{[\underline{\theta}_i,\overline{\theta}_i]}(\theta_i)$. The associated before-projection parameter error is as:

$$\chi_i \triangleq \alpha_i + \beta_i - \gamma_i. \tag{18}$$

Evidently, $\tilde{\theta}_i$ is related to χ_i via the following nonlinear relationship:

$$\tilde{\theta}_i = \frac{1}{2}\Delta\theta_i[\tanh(\chi_i+\gamma_i)-\tanh(\gamma_i)]. \tag{19}$$

By applying the control law described in (15), the closed-loop dynamics can be expressed as:

$$\dot{z} = -kz - b\sum_{i=1}^{N+1}\tilde{\theta}_i g_i(z,x,w). \tag{20}$$

Here, a proposition is presented to illustrate the manifold-attractivity attribute of the suggested NCE adaptive control strategy as well as facilitate the presentation of the main theorem in the sequel.

Proposition 1. If $z \in l^\infty$, the manifold defined by $\mathcal{W} \triangleq$

$\left\{(z,\tilde{\theta}_i,w)\in\mathbb{R}\times\mathbb{R}^{N+1}\times\mathbb{R}^m \middle| \sum_{i=1}^{N+1}\tilde{\theta}_i g_i(z,x,w)=0\right\}$ is an attractor.

Proof:

First off, we define a Lyapunov-like function:

$$V_\chi \triangleq |b|\sum_{i=1}^{N+1}\frac{\frac{1}{2}\Delta\theta_i \Xi(\chi_i)}{\varsigma_i}, \tag{21}$$

where,

$$\Xi(\chi_i)\triangleq \ln[\cosh(\chi_i+\gamma_i)]-\tanh(\gamma_i)\chi_i\,. \tag{22}$$

Showing that $\Xi(\chi_i)$ is a lower bounded scalar function is a straightforward task [15]. This leads to the conclusion that V_χ is also lower bounded. Differentiating $\Xi(\chi_i)$ with respect to χ_i yields:

$$\frac{\partial}{\partial\chi_i}\Xi(\chi_i)=\tanh(\chi_i+\gamma_i)-\tanh(\gamma_i)\,. \tag{23}$$

With this and (19), one can work out the time derivative of V_χ:

$$\dot{V}_\chi = |b|\sum_{i=1}^{N+1}\frac{\frac{1}{2}\Delta\theta_i}{\varsigma_i}\frac{\partial}{\partial\chi_i}\Xi(\chi_i)\dot{\chi}_i =$$

$$|b|\sum_{i=1}^{N+1}\frac{\frac{1}{2}\Delta\theta_i}{\varsigma_i}[\tanh(\chi_i+\gamma_i)-\tanh(\gamma_i)]\left(\dot{\alpha}_i+\dot{\beta}_i\right)$$

$$=|\beta|\sum_{k=1}^{N+M+1}\frac{\tilde{\theta}_k}{\gamma_k}\left(\dot{\alpha}_i+\dot{\beta}_i\right). \tag{24}$$

By invoking the parameter updating algorithms as proposed in (16), (24) can be further written carried out as:

$$\dot{\alpha}_i+\dot{\beta}_i=\begin{pmatrix}\frac{\partial\alpha_i}{\partial z}\\ \frac{\partial\alpha_i}{\partial x}\\ \frac{\partial\alpha_i}{\partial w}\end{pmatrix}^T\left(\begin{pmatrix}\dot{z}\\ \dot{x}\\ -\dot{w}\end{pmatrix}+\begin{pmatrix}kz\\ -\dot{x}\\ -\dot{w}\end{pmatrix}\right)$$

$$=-b\frac{\partial\alpha_i}{\partial x}\sum_{i=1}^{N+1}\tilde{\theta}_i g_i(z,x,w)\,. \tag{25}$$

The NCE proportional adaptation law for α_i as in (16) indicates that $\frac{\partial\alpha_i}{\partial x}=\varsigma_i\mathrm{sgn}(b)g_i(z,x,w)$, which yields:

$$\dot{\alpha}_i+\dot{\beta}_i=-\varsigma_i g_i(z,x,w)|b|\sum_{i=1}^{N+1}\tilde{\theta}_i g_i(z,x,w)\,. \tag{26}$$

At this point, $\dot{V}_\chi$ can be readily carried out as:

$$\dot{V}_\chi=-|b|\sum_{i=1}^{N+1}\tilde{\theta}_i g_i(z,x,w)\,|b|\left(\sum_{i=1}^{N+1}\tilde{\theta}_i g_i(z,x,w)\right)$$

$$=-b^2\left(\sum_{i=1}^{N+1}\tilde{\theta}_i g_i(z,x,w)\right)^2\le 0. \tag{27}$$

Given that V_χ is a lower bounded scalar function, it follows that $V_\chi,\chi_i,\tilde{\theta}_i\in L^\infty$. Plus, due to the negative semi-definiteness of $\dot{V}_\chi$, V_χ will converge to a finite constant $V_\chi(\infty)$. Next, the fact that $\int_0^\infty\dot{V}_\chi(t)dt=\left(V_\chi(0)-V_\chi(\infty)\right)\in L^\infty$ reveals the quadratic integrability of $\sum_{i=1}^{N+1}\tilde{\theta}_i g_i(z,x,w)$, namely, $\sum_{i=1}^{N+1}\tilde{\theta}_i g_i(z,x,w)\in L^2$. In addition, by examining the boundedness of $\ddot{V}_\chi$ (by utilizing the $z\in l^\infty$ condition), it can be concluded that $\frac{\partial}{\partial t}\sum_{i=1}^{N+1}\tilde{\theta}_i g_i(z,x,w)\in L^\infty$. By combining these observations with the corollary of Barbalat's Lemma, it can be eventually deduced that $\lim_{t\to\infty}\sum_{i=1}^{N+1}\tilde{\theta}_i g_i(z,x,w)=0$ so that $\mathcal{W}$ is indeed attractive. ■

Proposition 1 forms the basis for proving the following theorem.

Theorem 1. The adaptive closed-loop system composed of (10), (15), and (16) is globally stable with the following characteristics: **a)** $\forall t\in\mathbb{R}^+,\varphi_l(t)<e(t)<\varphi_u(t)$ and $\lim_{t\to\infty}z(t),e(t)=0$; **b)** The extended state-space $(z,\tilde{\theta}_i)\in\mathbb{R}\times\mathbb{R}^{N+1}$ will be attracted to the manifold $\mathcal{W}$ defined in Proposition 1; **c)** Regardless of the adaptation, $\hat{\theta}_i$ are strictly confined within pre-estimated $\left[\underline{\theta}_i,\overline{\theta}_i\right]$.

Proof:

We consider the following lower-bounded, Lyapunov-like function V composed of a quadratic term respecting z and V_χ defined in Proposition 1:

$$V=\frac{1}{2}z^2+\varepsilon V_\chi, \tag{28}$$

where $\varepsilon\in\mathbb{R}_+$. The derivative of V with respect to time along the trajectory of (20) can be rolled out as:

$$\dot{V}=-kz^2-zb\sum_{i=1}^{N+1}\tilde{\theta}_i g_i(z,x,w)+\varepsilon\dot{V}_\chi$$

$$\le -kz^2+|z|\left|b\sum_{i=1}^{N+1}\tilde{\theta}_i g_i(z,x,w)\right|$$

$$-\varepsilon b^2\left(\sum_{i=1}^{N+1}\tilde{\theta}_i g_i(z,x,w)\right)^2. \tag{29}$$

The inequality in (29) is a result of Proposition 1 and the Cauchy-Schwarz inequality.

To facilitate the subsequent analysis, we choose ($\varepsilon_s\in\mathbb{R}_+$):

$$\varepsilon=\varepsilon_s+\frac{\sqrt{2}}{\sqrt{k}}, \tag{30}$$

which leads to:

$$\dot{V}\le -kz^2-\mathcal{M}^2-\varepsilon_s b^2\left(\sum_{i=1}^{N+1}\tilde{\theta}_i g_i(z,x,w)\right)^2$$

$$\le -kz^2-\varepsilon_s b^2\left(\sum_{i=1}^{N+1}\tilde{\theta}_i g_i(z,x,w)\right)^2. \tag{31}$$

In (31), $\mathcal{M}^2=\left(|z|\sqrt{\frac{k}{2}}-\frac{1}{2}|b|\left|\sum_{i=1}^{N+1}\tilde{\theta}_i g_i(z,x,w)\right|\sqrt{\frac{2}{k}}\right)^2$ results from the completion of the square. $\dot{V}\le 0$ immediately demonstrates that the closed-loop system is globally stable, and all signals are bounded. Thus, the boundedness of z reveals the realization of the PPC objective ($\forall t\in\mathbb{R}^+,\varphi_l(t)<e(t)<\varphi_u(t)$), which ensures the guaranteed prescribed transient behavior of the tracking error e. Besides, we can conclude that $\lim_{t\to\infty}z(t),e(t),\sum_{i=1}^{N+1}\tilde{\theta}_i g_i(z,x,w)=0$ by following the standard signal boundedness and convergence analysis (as conducted in proving Lemma 1). Therefore, we show that the error-tracking error can be rendered zero in the face of parametric uncertainties, and the extended state-space $(z,\tilde{\theta}_i)\in\mathbb{R}\times\mathbb{R}^{N+1}$ will converge to the

manifold $\mathcal{W}$. Last but not least, the smooth projection operator ascertains that $\hat{\theta}_k \in [\underline{\theta}_k, \overline{\theta}_k]$. The proof for Theorem 1 is now complete. ■

Remark 3: The proposed NCE adaptive PPC scheme offers two key attributes for respecting transient performance. First and foremost, the tracking error is strictly confined to a prescribed exponentially converging funnel, which offers the guaranteed transient performance to the closed-loop adaptive system. The second major attribute of the proposed control strategy is its ability to achieve arbitrarily fast asymptotic convergence of parameter error-induced term $\sum_{i=1}^{N+1} \tilde{\theta}_i g_i(z, x, w)$, with the convergence speed tunable by ς_i. This leads to the prompt recovery of desired (exponentially stable) deterministic closed-loop dynamics, which fosters a superior transient performance.

III. Application To GFM Design

A. Vehicle Planar Dynamics

Ground vehicles equipped with torque vectoring feature independent torque and active steering controls for all wheels. In this paper, we consider a four-wheel vehicle (e.g., a sedan) whose planar vehicle dynamics can be modeled as [1] (assuming negligible pitch and roll motion):

$$\frac{d}{dt}\begin{pmatrix} v_x \\ v_y \\ \omega_z \end{pmatrix} = \begin{pmatrix} v_y\omega_z - \frac{\rho}{2M} C_d A_f v_x^2 \\ -v_x\omega_z \\ 0 \end{pmatrix} + \Lambda \begin{pmatrix} F_x \\ F_y \\ M_z \end{pmatrix}, \tag{32}$$

where $\Lambda = \mathrm{diag}(M^{-1}, M^{-1}, I_{zz}^{-1})$. In (32), v_x, v_y, and ω_z are the vehicle's longitudinal and lateral velocities and yaw rate (all in the vehicle body-fixed frame), respectively. M and I_{zz} are vehicle mass and yaw inertia, respectively. ρ, C_d, and A_f are parameters associated with longitudinal aerodynamic resistance. F_x, F_y, and M_z are generalized longitudinal and lateral forces and yaw moment, respectively, which are treated as virtual controls to the planar vehicle dynamic model. In practice, v_x and ω_z are "cheap" to be measured via sensors (e.g., IMU). v_y, on the other hand, should be estimated with observers/estimators.

B. GFM Governor Design

Since the system is fully actuated, *i.e.*, the number of control inputs equal to the number of states, we can decouple it into three single-input–single-output (SISO), nonlinear, first-order systems, namely,

$$\begin{cases} \dot{v}_x = a_{x1} f_{x1}(v_y, \omega_z) + a_{x2} f_{x2}(v_x) + b_x F_x \\ \dot{v}_y = a_y f_y(v_x, \omega_z) + b_y F_y \\ \dot{\omega}_z = b_z M_z \end{cases}, \tag{33}$$

where $a_{x1} = a_y = 1$, $a_{x2} = \frac{\rho}{2M} C_d A_f$, $b_x = b_y = M^{-1}$, $b_z = I_{zz}^{-1}$, $f_{x1} = v_y\omega_z$, $f_{x2} = -v_x^2$, and $f_y = -v_x\omega_z$. At this point, we notice that the first-order dynamics in (33) are written in the form as in (1). Therefore, one can readily exploit the theoretical result derived in Section II to design the GFM governor to control vehicle motion signals v_x, v_y, and ω_z. For illustration, we will present the design for the vehicle yaw rate controller here. In a nutshell, we desire ω_e (the yaw rate tracking error) to be regulated within the funnel $|\omega_e(t)| \triangleq |\omega_z(t) - r_\omega(t)| < \varphi_z(t), \forall t \in \mathbb{R}^+$ where $\varphi_z(t) = (\varphi_{z0} - \varphi_{z\infty})\exp(-\kappa_z t) + \varphi_{z\infty}$ and $r_\omega(t)$ is the reference yaw rate (sufficiently smooth). To enforce such a control objective in spite of the parametric uncertainty stemming from I_{zz} (which almost always presents due to vehicular payload and weight distribution variations), the following NCE adaptive PPC strategy is enforced to generate the desired generalized yaw moment command:

$$M_z = -\hat{\theta}_z g_z(z_z, \omega_z, r, \dot{r}). \tag{34}$$

In (34),

$$g_z(z_y, v_x, \omega_z) = \frac{-\dot{r}_\omega(t) - \omega_e\dot{\varphi}_z\varphi_z^{-1} + \zeta_z}{\varphi_z(t)(1 - \omega_e^2\varphi_z^{-2})}, \tag{35}$$

where $\zeta_z = \varphi_z(1 - \omega_e^2\varphi_z^{-2})k_z z_z$ and $z_z = \frac{1}{2}\ln\left(\frac{1+\omega_e\varphi_z^{-1}}{1-\omega_e\varphi_z^{-1}}\right)$. Besides, the $\hat{\theta}_z$ is updated via:

$$\begin{cases} \hat{\theta}_z = \Pi_{[\underline{\theta}_z, \overline{\theta}_z]}(\alpha_z + \beta_z) \\ \alpha_z = \varsigma_z \mathrm{sgn}(b_z) \int_0^{z_z} g_z(\varsigma, \omega_z, r, \dot{r}) d\varsigma \\ \dot{\beta}_z = \begin{pmatrix} \frac{\partial \alpha_z}{\partial z_z} & \frac{\partial \alpha_z}{\partial \omega_z} & \frac{\partial \alpha_z}{\partial r} & \frac{\partial \alpha_z}{\partial \dot{r}} \end{pmatrix} \begin{pmatrix} k_z z_z \\ -\dot{\omega}_z \\ -\dot{r} \\ -\ddot{r} \end{pmatrix} \end{cases}, \tag{36}$$

where $\varsigma_z, k_z \in \mathbb{R}_+$ are design parameters. The GFM governor based on such a control design can ensure both the prescribed transient performance as well as the recovery of the desired deterministic behavior of the closed-loop vehicle yaw dynamics despite the uncertain parameter b_z.

Remark 4: Although not presented here, the same procedure can be straightforwardly extended to design governing laws to control the vehicle's longitudinal and lateral velocities (which will produce desired generalized longitudinal and lateral force commands).

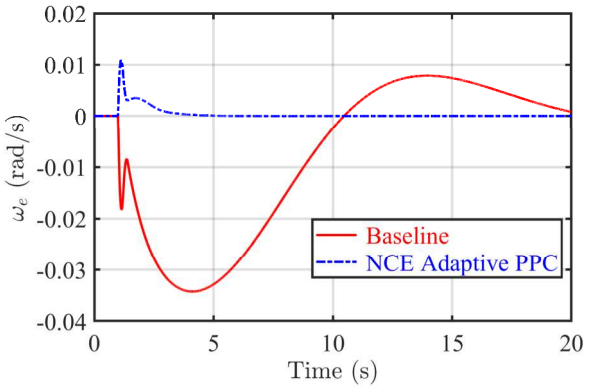

Figure 1. Reference step yaw rate tracking comparison.

IV. Simulation Study

In this section, results from the ASM-based simulation study are presented to justify the proposed control strategy (ASM employed here is a high-fidelity simulation software widely utilized in the automotive industry to simulate different aspects of vehicle behavior and performance). For demonstration, we will control the vehicle to track both step (whose magnitude is $0.5\,rad/s$) and sinusoidal yaw rate (with an amplitude of $0.5\,rad/s$ and a frequency of $0.5\,Hz$) commands at a cruising speed of $25\,m/s$. The reference for v_y is zero. We will compare our NCE adaptive PPC with a baseline quadratic-Lyapunov-function-based MRAC from [7]. We adopt the solution in [5] as the control allocation scheme that distributes the GFM commands to actuators. The prescribed funnel function for the yaw rate tracking error is specified as $\varphi_z(t) = 0.03\exp(-0.1t) + 0.01$. The $\hat{\theta}_z$ is

initialized based on $\hat{I}_{zz} = 1800\ kg \cdot m^2$ whereas the ground truth is $I_{zz} = 2000\ kg \cdot m^2$. The projection bound for $\hat{\theta}_z$ is set as $[1/2500, 1/1500]$.

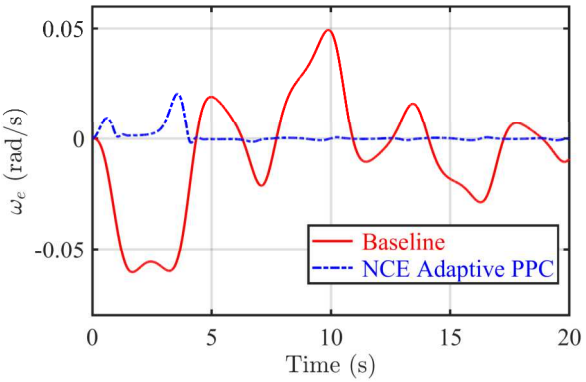

Figure 2. Reference sinusoidal yaw rate tracking

As demonstrated in Figures 1 and 2, both the NCE adaptive PPC and the baseline controller have been effective in stabilizing the closed-loop systems for both step and sinusoidal yaw rate tracking. However, our approach has demonstrated superior performance compared to the baseline strategy in several aspects. Evidently, the NCE adaptive PPC exhibits significantly better transient performance. Our solution strictly confines ω_e within the prescribed funnel, leading to the prompt convergence of the yaw rate tracking error. On the contrary, the baseline controller, while able to stabilize the error dynamics, exhibits poor transient performance as evidenced by the slow and oscillatory convergence of ω_e.

V. Conclusion

This paper articulates a novel control approach that combines PPC, NCE adaptive control design, and a hyperbolic tangent function-based smooth projection operator. The proposed control strategy is exploited to design the GFM governor for torque vectoring in ground vehicles. The suggested solution has a significant advantage in ensuring guaranteed transient performance and recovery of the deterministic desired behavior of the closed-loop adaptive system, even in the presence of parametric uncertainties. The efficacy of the proposed control strategy is validated through simulations using ASM, and its superiority over a baseline adaptive control solution is demonstrated. Future studies will focus on experimenting with the proposed GFM governor using real vehicles. Further, the theoretical findings will be extended to systems with higher orders and other canonical structures.

References

[1] J. Wang and R. G. Longoria, "Coordinated and reconfigurable vehicle dynamics control," *IEEE Trans. Contr. Syst. Technol.*, vol. 17, no. 3, pp. 723–732, May 2009, doi: 10.1109/TCST.2008.2002264.

[2] L. Xiong et al., "IMU-Based Automated Vehicle Body Sideslip Angle and Attitude Estimation Aided by GNSS Using Parallel Adaptive Kalman Filters," *IEEE Trans. Veh. Technol.*, vol. 69, no. 10, pp. 10668–10680, Oct. 2020, doi: 10.1109/TVT.2020.2983738.

[3] Z. Wang, X. Zhou, and J. Wang, "Extremum-Seeking-Based Adaptive Model-Free Control and Its Application to Automated Vehicle Path Tracking," *IEEE/ASME Trans. Mechatron.*, vol. 27, no. 5, pp. 3874–3884, Oct. 2022, doi: 10.1109/TMECH.2022.3146727.

[4] O. Temiz, M. Cakmakci, and Y. Yildiz, "A Fault Tolerant Vehicle Stability Control Using Adaptive Control Allocation," in *ASME 2018 Dynamic Systems and Control Conference (DSCC)*, Atlanta, Georgia, USA, Sep. 2018, p. V001T09A002. doi: 10.1115/DSCC2018-8976.

[5] R. Wang, C. Hu, F. Yan, and M. Chadli, "Composite Nonlinear Feedback Control for Path Following of Four-Wheel Independently Actuated Autonomous Ground Vehicles," *IEEE Trans. Intell. Transport. Syst.*, vol. 17, no. 7, pp. 2063–2074, Jul. 2016, doi: 10.1109/TITS.2015.2498172.

[6] X. Chen, K. Zhou, and Y. Tan, "Revisit of LQG Control–A New Paradigm with Recovered Robustness," in *2019 IEEE 58th Conference on Decision and Control (CDC)*, Nice, France, Dec. 2019, pp. 5819–5825. doi: 10.1109/CDC40024.2019.9030062.

[7] X. Zhou, Z. Wang, and J. Wang, "Automated Vehicle Path Following: A Non-Quadratic-Lyapunov-Function-Based Model Reference Adaptive Control Approach With C^∞-Smooth Projection Modification," *IEEE Trans. Intell. Transport. Syst.*, vol. 23, no. 11, pp. 21653–21664, Nov. 2022, doi: 10.1109/TITS.2022.3182928.

[8] M. K. Ghezzi, A. Doria-Cerezo, and J. M. Olm, "Yaw moment MRAC with optimal torque vectoring for a four in-wheel motor EV," in *2018 IEEE International Conference on Industrial Technology (ICIT)*, Lyon, France, Feb. 2018, pp. 1820–1825. doi: 10.1109/ICIT.2018.8352460.

[9] L. Zhang *et al.*, "An Adaptive Backstepping Sliding Mode Controller to Improve Vehicle Maneuverability and Stability via Torque Vectoring Control," *IEEE Trans. Veh. Technol.*, vol. 69, no. 3, pp. 2598–2612, Mar. 2020, doi: 10.1109/TVT.2019.2950219.

[10] M. Chae, Y. Hyun, K. Yi, and K. Nam, "Dynamic Handling Characteristics Control of an in-Wheel-Motor Driven Electric Vehicle Based on Multiple Sliding Mode Control Approach," *IEEE Access*, vol. 7, pp. 132448–132458, 2019, doi: 10.1109/ACCESS.2019.2940434.

[11] H. Ma, Q. Zhou, H. Li, and R. Lu, "Adaptive Prescribed Performance Control of A Flexible-Joint Robotic Manipulator With Dynamic Uncertainties," *IEEE Trans. Cybern.*, vol. 52, no. 12, pp. 12905–12915, Dec. 2022, doi: 10.1109/TCYB.2021.3091531.

[12] M. R. Akella, "Adaptive Control—A Departure from the Certainty-Equivalence Paradigm," *J of Astronaut Sci*, vol. 52, no. 1–2, pp. 75–91, Mar. 2004, doi: 10.1007/BF03546422.

[13] X. Zhou, H. Shen, Z. Wang, H. Ahn, and J. Wang, "Driver-Centric Lane-Keeping Assistance System Design: A Noncertainty-Equivalent Neuro-Adaptive Control Approach," *IEEE/ASME Trans. Mechatron.*, pp. 1–12, 2023, doi: 10.1109/TMECH.2023.3236245.

[14] Z. Cai, M. S. deQueiroz, and D. M. Dawson, "A Sufficiently Smooth Projection Operator," *IEEE Trans. Automat. Contr.*, vol. 51, no. 1, pp. 135–139, Jan. 2006, doi: 10.1109/TAC.2005.861704.

[15] X. Zhou, Z. Wang, H. Shen, and J. Wang, "Systematic Synthesis of a Class of Smooth Parameter Projection Operators for Stable Adaptive Systems," *ASME Letters in Dynamic Systems and Control*, vol. 2, no. 3, p. 031009, Jul. 2022, doi: 10.1115/1.4055082.

[16] C. Hu and J. Wang, "Trust-Based and Individualizable Adaptive Cruise Control Using Control Barrier Function Approach with Prescribed Performance," *IEEE Transactions on Intelligent Transportation Systems*, 23(7), pp. 6974 – 6984, 2022, doi: 10.1109/TITS.2021.3066154.